J Mater Sci (2023) 58:1293–1304

Metals & corrosion

Improvement of interface stability and anti-friction performance of anodized AA6082 alloys by adjusting the state of Mg before anodization

Wenbo Zhu[1], Yunlai Deng[1,2], Chaojie Liang[1], Chenglei Wang[3], Xiaobin Guo[1], and Xuehong Xu[2,*]

[1] School of Materials Science and Engineering, Central South University, Changsha 410083, Hunan, China
[2] Light Alloy Research Institute, Central South University, Changsha 410083, Hunan, China
[3] School of Materials Science and Engineering, and Guangxi Key Laboratory of Information Materials, Guilin University of Electronic Technology, Guilin 541004, Guangxi, China

Received: 20 September 2022
Accepted: 30 November 2022
Published online: 1 January 2023

ABSTRACT

A change in the heat treatment state of aluminum matrix before anodization was used to change the state of Mg in this work. The effects of Mg on the interface structure of the film/substrate of anodized AA6082 alloys were systematically studied when Mg existed in the state of Mg_5Si_6, supersaturated solid solution, and atomic clusters or GP zones. The cross-sectional morphology and film/aluminum alloy interface structure of the oxide film were characterized by SEM and HRTEM, respectively, and the reciprocating friction test was used to compare and analyze the effect of different film/aluminum alloy interface structures on the friction resistance of the oxide film. The results show that the state of Mg before anodization plays a key role in the stability of the film/aluminum alloy interface after anodization, which also has an important impact on the wear performance. Before anodization, the anodized AA6082 alloys have the best friction resistance when the Mg exists in atomic clusters or GP zones, follow by the supersaturated solid solution, and the last is the β″ phase.

Introduction

The advantages of aluminum alloys include low density, good weldability, good moldability and excellent overall mechanical properties, making them widely used in automobiles, rail transit, aerospace and other fields. It is known that 6xxx aluminum alloys exhibit significant mechanical properties, formability, better weldability and lower production costs relative to 2xxx and 7xxx series aluminum alloys [1]. However, low hardness and poor wear resistance limit its application range [2, 3]. Surface modification technology was widely used to improve

Handling Editor: Naiqin Zhao.

Address correspondence to E-mail: xuehongxu@csu.edu.cn

https://doi.org/10.1007/s10853-022-08056-0

the friction resistance of materials to meet the use requirements of various materials under friction conditions [4]. Anodizing technology is one of the most commonly used surface modification technologies for aluminum alloys [5–8]. Some studies have shown that when the hard anodizing process is used to strengthen the surface of the aluminum alloys, a thick oxide film will be formed, which has high hardness, excellent corrosion resistance and good wear resistance. [9, 10].

Although the friction property of aluminum alloys has been improved to a certain extent after anodizing, it still cannot meet the practical application requirements due to the large friction coefficient [11]. Numerous studies have been conducted in order to achieve this goal. Benefiting from the uniform and ordered nanoscale pores formed during the anodization process [12, 13], these nanoporous structures can serve as reservoirs for lubricants and abrasive particles. Wang et al. [14] found that adding perfluoropolyether (PFPE) and octadecyltrichlorosilane (OTS) into the anodic oxide film can effectively reduce the friction coefficient of the oxide film and improve the wear life. In addition, the friction coefficient of the oxide film can also be effectively reduced by adding some abrasive particles into the oxide film, such as MoS_2, carbon nanofibers and iodide, etc. [15–17]. Skeldon et al. [16] reanodized the sample in 10^{-2} M ammonium tetrathiomolybdate electrolyte and found that the oxide film contained MoS_2. Compared with no self-lubricating film, the wear coefficient decreased from 3.5×10^{-10} m^2 to 4×10^{-12} m^2. Takayav et al. [18] found that the friction coefficient of the oxide film could be reduced from 0.8 to 0.4 by forming 0.1% iodide in the pores of the oxide film. Therefore, adding lubricating particles into the nano-pores of the oxide film is a fast and effective method to reduce the friction coefficient of the oxide film. Kim et al. [19] found that the friction coefficient of oxide film was related to its pore size and loading load, when the oxide film on the friction coefficient was dominant at relatively high loads (0.1 N and 1 N): the larger the pore size, the higher the friction coefficient. In addition, studies have shown that the oxide film porosity, as well as the pore depth and pore diameter ratio, also affects the friction resistance of the oxide film. These can be obtained by changing the anodizing process to obtain the optimal porosity as well as the ratio of pore depth and pore diameter, thereby improving the friction resistance of the oxide film [19, 20].

The above studies provide an important basis for anodizing in improving the wear resistance of aluminum alloys, but these studies are all through changing the surface state of the oxide film to improve the wear resistance. Since the film/aluminum alloy interface needs to withstand the cyclic contact stress during the friction process, and the elastic modulus and hardness of the oxide film are quite different from those of the aluminum matrix. Once the strength and toughness of the film/aluminum alloy interface cannot resist the effect of cyclic contact stress, the aluminum matrix would deform, which causes fatigue and adhesive wear, reducing the wear resistance. The film/aluminum alloy interface structure on the friction resistance is very important. Because the anodization process is an electrochemical reaction, aluminum is converted into Al^{3+} during the oxidation process [21–23]. For Al–Mg–Si alloy, Mg will preferentially ionize and participate in the oxidation reaction during the anodization process since Mg has higher chemical activity than Al [24]. In general, the precipitation sequence of Al–Mg–Si alloys is assumed to be as follows: Supersaturated solid solution → Atomic clusters → GP zones → β″ → U1, U2, B′, β′ → β [25–30]. The consumption of Mg during the anodizing process is different due to the state of Mg in Al–Mg–Si alloys in different heat treatment states, thereby affecting the oxide film/aluminum alloy interface. However, the influence of different states of Mg on the structure of the film/aluminum alloy interface is still unclear.

To sum up, the wear resistance of 6xxx series aluminum alloy after anodic oxidation is improved mainly by regulating the anodic oxidation process, or by adding grinding particles, but the substrate/film interface structure on the influence of the wear resistance is still unclear. The purpose of this study is to further improve the wear resistance of the overall material by adjusting the stability of the substrate/film interface structure without changing the high wear resistance of the anodized film and the properties of the base material. In this study, the AA6082 alloy will be subjected to different heat treatments to change the state of Mg before anodization. The effects of Mg in three different states (precipitates, supersaturated solid solutions, atomic clusters or GP zones) on the interfacial structure of

the film/substrate after anodic oxidation were systematically studied. The SEM and HRTEM were used to characterize the cross-sectional morphology of the oxide film and the structure of the film/aluminum alloy interface. The effects of different film/aluminum alloy interface structures on the wear resistance of the oxide film were compared and analyzed by the reciprocating friction test. All the samples in this study were prepared under industrial conditions, and the test results are of great significance for improving the protective properties of aluminum alloys used in rail transit and automobiles.

Experimental

Materials and anodizing

AA6082 alloy commercial plate with 6 mm thickness was used for this research, and the alloy composition is shown in Table 1.

In order to ensure that this study meets the industrial demand, we selected the most common heat treatment process of the AA6082 alloys (T6, heat preservation at 530 °C for 1 h and aging at 170 °C for 6 h). Before anodizing, the hot-rolled AA6082 samples were solution treated at 530 °C for 1 h, followed by water quenching. These samples were divided into three categories: In the first type, the solid solution samples were directly anodized, followed by artificial aging at 170 °C for 6 h (marked as S-AO). In the second type, the samples in the solid solution state were artificially aged at 170 °C for 1 h, followed by anodization, and finally artificially aged at 170 °C for 5 h (marked as U-AO). In the third type, the solid solution samples were artificially aged at 170 °C for 6 h, followed by anodization (marked as P-AO). The specific process flow is shown in Fig. 1. The same anodizing process was used for the samples in different heat treatment states in this study, which was consistent with our previous research [31, 32]. Anodizing was performed in a 10% sulfuric acid solution at − 3 °C. The segmented constant voltage method was adopted, the voltage ranged from 14 to 28 V, and the time was 65 min. Finally, seal the hole with boiling water for 10 min.

Table 1 Composition of AA6082 alloy, wt%

Element	Si	Fe	Zn	Mg	Cr	Mn	Ti	Al
Content	0.58	0.31	0.10	1.09	0.17	0.61	0.09	Bal

Test and characterization

The friction test was carried out on the HSR-2M reciprocating friction tester under a load of 3 N and a frequency of 30 Hz for 20 min. The grinding material is the Si_3N_4 ball with a diameter of 3 mm. The schematic diagram of reciprocating friction test is shown in Fig. 2. In order to ensure the accuracy of friction test results, three parallel samples were used for each group of tests under the same conditions.

Scanning electron microscopy (SEM, Zeiss Evo Ma10, 20 kV accelerating voltage) was used to characterize the cross-sectional morphologies of the three films and the Transmission electron microscopy (TEM) observations of wear morphology. The TEM observations were performed using a Tecnai-G2-F20 operated at 200 kV. TEM foils of film/substrate interface were prepared by focused ion beam (FIB, FEI Helios NanoLab 600i).

Results

SEM images of the film/matrix

The cross-sectional morphologies of the three films were observed by SEM as shown in Fig. 3. The thickness of the three films is about 20 μm, indicating that there is no impact on film thickness after the same anodizing process for the aluminum alloy samples in different treatment heat states. Besides, there are some microscale pores that can be seen in all films, which are caused by the coarse phases. As an inert phase, Al–Fe–Mn–Si is the most common coarse phases in Al–Mg–Si alloys. During anodization, the aluminum matrix around the coarse phase is preferentially dissolved and oxidized, resulting in the exfoliation of the particles, and some exfoliated particles would remain in the oxide film, leading to the formation of pores [33, 34]. The coarse phases cannot be eliminated by heat treatment processes since they are the primary phases of the alloys.

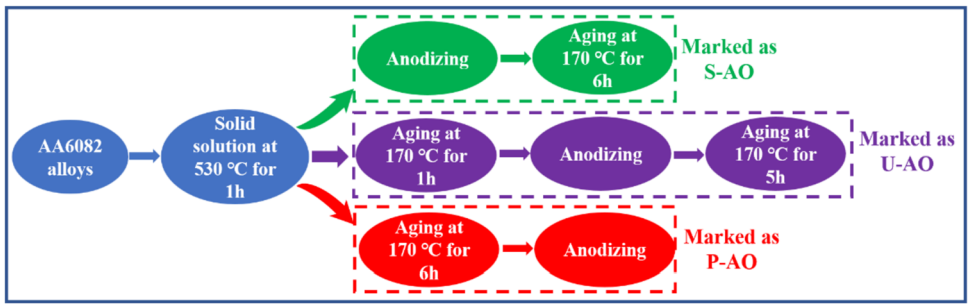

Figure 1 Flowchart of heat treatment and anodizing process of AA6082 alloy.

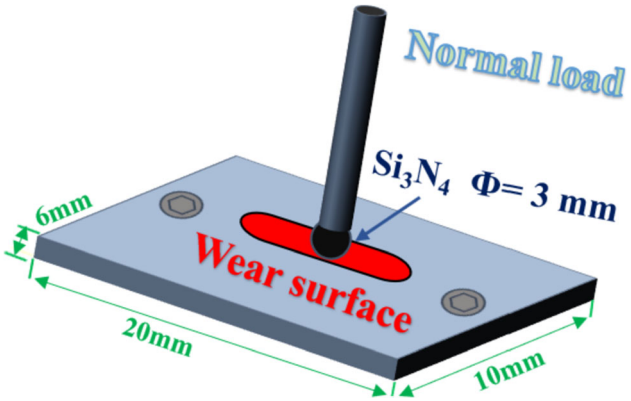

Figure 2 Schematic diagram of reciprocating friction test.

TEM images of the film/matrix interface

To furtherly explore the influence of the different heat treatment states of aluminum alloy before anodization on the film/aluminum alloy interface, a transmission electron microscope (TEM) was performed. Figure 4a–c are the TEM bright-field images of the film/aluminum alloy interface of the P-AO, U-AO and S-AO samples acquired from the $[100]_{Al}$ zone axis, respectively. Needle-like precipitates could be found in the three diagrams, but the quantity, density and size of the precipitates at the U-AO film/aluminum alloy interface (Fig. 4a) are higher than those of the P-AO film and S-AO film (as shown in Fig. 4a, c). In addition, needle-shaped particles are densely distributed outside the 50 nm range of the S-AO film boundary, while the P-AO and U-AO film/matrix has needle-shaped particles in the entire field of view. In order to further explain the above situation, HRTEM images were taken out.

Figure 5a–c shows the HRTEM images of the film/aluminum alloy interface of the P-AO, U-AO and S-AO samples acquired from the $[110]_{Al}$ zone axis, respectively. Some needle-like precipitates can be found at the interface of the P-AO and U-AO samples, which are preliminarily determined to be Mg_xSi_y. To further confirm the type of this precipitated phase, we prepared high-resolution samples by electrolysis-double jet on the same sample, and took HRTEM imaging under the $[100]_{Al}$ zone axis (Fig. 6a). Figure 6b depicts the fast Fourier transformation (FFT) image acquired from Fig. 6a. It is concluded that the type of the precipitates is β″ phase (Mg_5Si_6) through lattice calibration. Interestingly, compared with the P-AO and U-AO samples, no β″ phase was found at the interface of the S-AO sample. Research shows that Mg would preferentially ionize and participate in the oxidation reaction during the anodization process due to its higher chemical activity [24]. For the S-AO sample, because Mg was dispersed in the aluminum matrix before anodization, which would easily cause the Mg distributed on the surface of the aluminum alloy to be exhausted during the anodization process, resulting in the

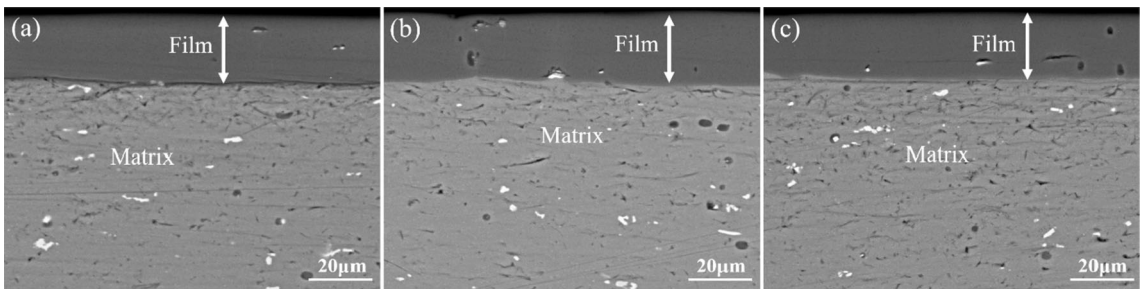

Figure 3 SEM images of the cross-sectional morphology of the oxide film. **a** P-AO film, **b** U-AO film and **c** S-AO film.

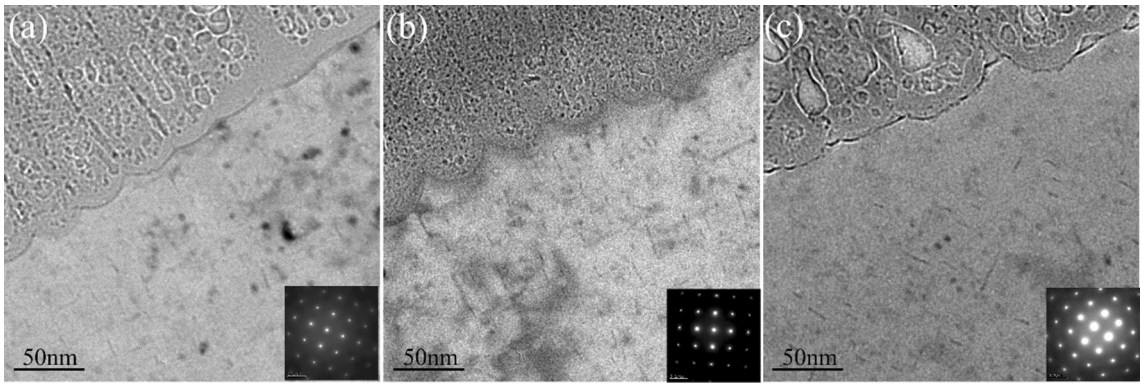

Figure 4 **a**–**c** as the interface TEM Bright-field images of P-AO, U-AO and S-AO films, respectively.

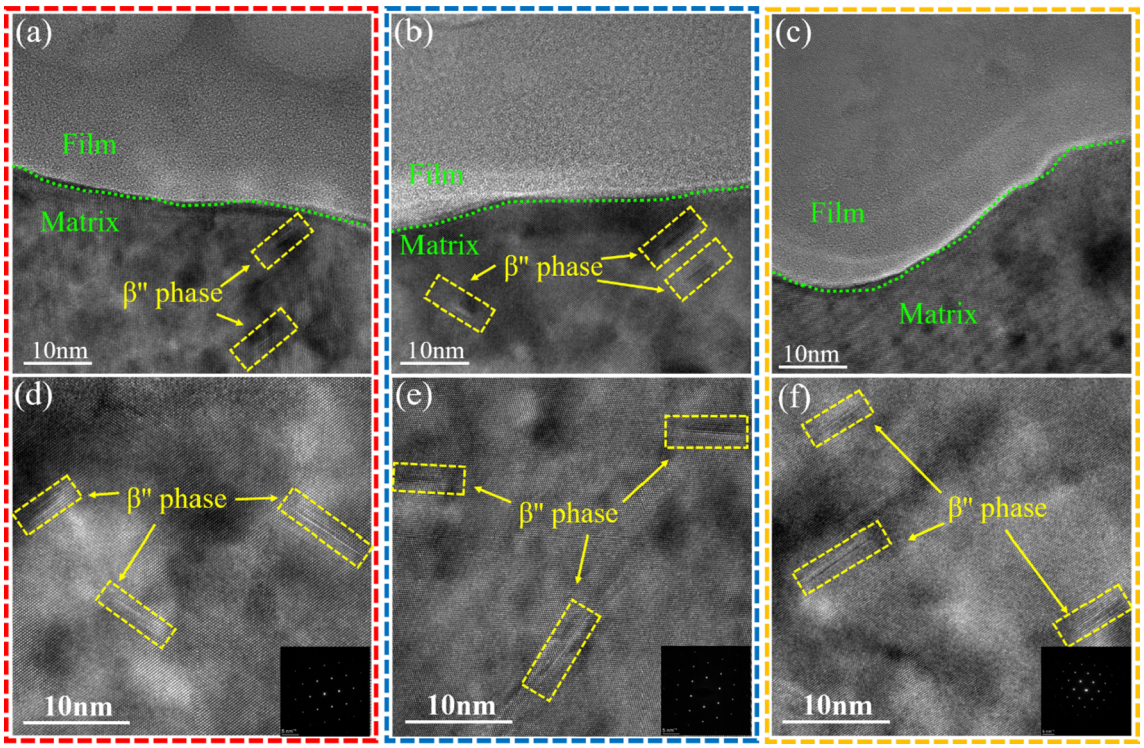

Figure 5 **a**–**c** HRTEM images of film/aluminum alloy interface of P-AO, U-AO and S-AO samples, respectively; **d**–**f** HRTEM images of aluminum matrix of P-AO, U-AO and S-AO samples, respectively.

formation of an Mg-poor region at the film/aluminum alloy interface. As a result, during the subsequent artificial aging process, the β″ phase cannot be formed at the film/aluminum alloy interface. Different from the S-AO sample, the U-AO sample was artificially aged at 170 °C for 1 h before the anodization treatment, the Mg at this time did not exist in the state of precipitation. The study shows that for Al–Mg–Si alloy, Mg mainly forms the GP zones after artificial aging at 170 °C for 2 h [35, 36]. According to the precipitation sequence of the Al–Mg–Si alloy [25–30], the Mg at this state mainly forms atomic clusters or GP zones. Although Mg consumption also occurs during anodization, a certain amount of Mg still exists in these zones after anodization, this is because a large amount of Mg is enriched in atomic clusters or GP zones. Therefore, throughout the aging process, some regions that meet the conditions would be transformed to the β″ phase.

HRTEM was also used to determine the influence of the heat treatment state before anodization on the β″ precipitates of the aluminum matrix at the non-

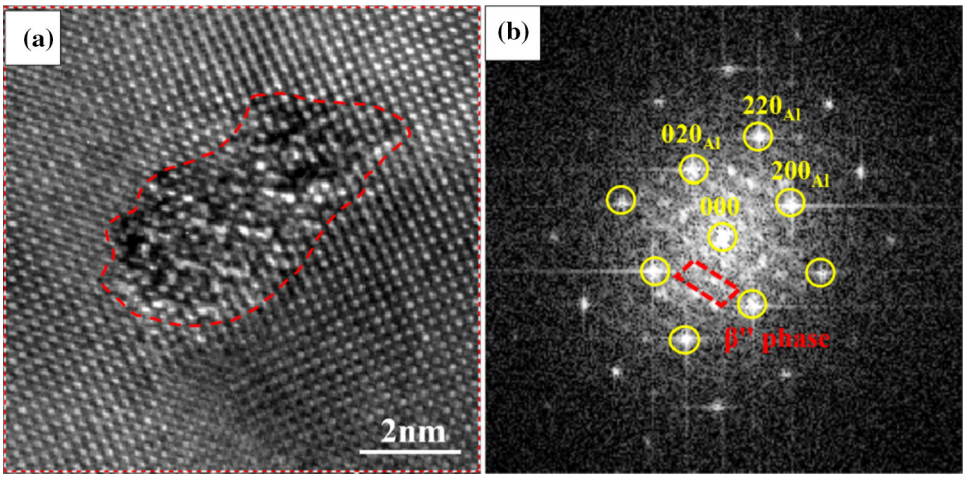

Figure 6 **a** HRTEM image of aluminum matrix of P-AO sample under $[100]_{Al}$ zone axis; **b** FFT image acquired from figure (**a**).

interface. Figure 5d–f are the HRTEM images of aluminum matrix at non-interface of the P-AO, U-AO and S-AO samples acquired from the $[110]_{Al}$ zone axis, respectively. It can be seen that within the same field of view, there are the same number of β″ precipitates in the aluminum matrix at non-interface of the three samples, and the size and dispersion degree of the precipitates are similar. This also shows that the strength of the aluminum matrix at non-interface is similar. To sum up, the heat treatment state of the aluminum alloy before anodization only affects the precipitation phase of the aluminum matrix at the interface, and does not affect the overall aluminum alloy.

Friction properties

It can be known that the film/aluminum alloy interface structure of aluminum alloy materials in different heat treatment states is different after anodizing treatment from analysis of "TEM images of the film/matrix interface" section. To explore the effects of these different film/aluminum alloy interface structures on the friction properties, the reciprocating friction test was carried out. Figure 7 shows the friction coefficient curves of the P-AO, U-AO and S-AO and only anodized without aging samples. The friction coefficient of the four films shows different trends. For the P-AO sample, in the initial stage of friction, the friction coefficient rises rapidly, and when the friction time reaches 2.5 min, the friction coefficient shows a relatively stable trend, and the average friction coefficient at this time is about 0.08. However, it is worth noting that compared with the P-AO sample, the time for the friction coefficient

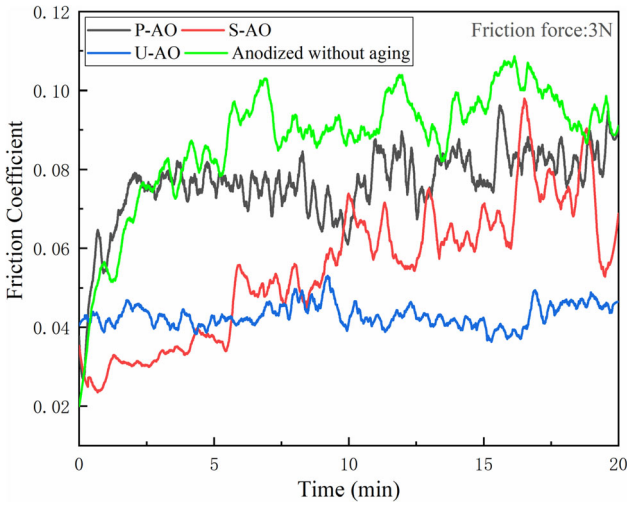

Figure 7 Friction coefficient curve.

curve of the S-AO sample to enter the flat stage is more delayed. After about 6 min, the friction coefficient increases rapidly from 0.04. Different from the P-AO and S-AO samples, the friction coefficient of the U-AO sample shows a relatively stable trend in the whole friction process, and does not increase rapidly, and the friction coefficient remains around 0.04. In order to further investigate the influence of heat treatment state on the tribological properties of anodized samples, the only anodized without aging samples were tested under the same conditions. For the only anodized without aging sample, the variation trend of the friction coefficient curve is similar to that of P-AO, but the friction coefficient is slightly higher.

To explore the mechanisms for the difference in friction coefficient of the four films, the friction morphologies of the four films were observed and

analyzed by SEM as shown in Fig. 8. Lots of cracks appear on the surface of the four films after the reciprocating friction test. This is because the anodic oxide film belongs to the alumina ceramic film, which is relatively brittle, so the film will break rapidly under the action of contact compressive stress. It can be seen that after a 20 min reciprocating friction test of the P-AO sample, a large number of cracks, large debris accumulation areas and some small holes appear on the surface (as shown in Fig. 8a). This indicates that the specimen is subjected to serious fatigue wear and adhesive wear. However, unlike the P-AO sample, only some cracks are observed in the film after the U-AO sample is rubbed back and forth (as shown in Fig. 8b). This indicates that the oxide film is well combined with the aluminum alloy substrate, and the film/aluminum alloy interface has sufficient toughness to resist cyclic contact stress.

According to the friction coefficients of the four films in Fig. 7, the friction coefficient of the S-AO sample is low in the first 5 min, and then rises rapidly. To explore the reasons for this phenomenon, we carried out SEM friction morphology characterization of S-AO sample after 5 min and 20 min reciprocating friction, respectively (as shown in Fig. 8c, d). When the S-AO sample is subjected to a 5 min reciprocating friction test, only some cracks are observed on the surface of the oxide film, and the results are similar to those of the U-AO sample. When the S-AO sample is subjected to a 20 min reciprocating friction test, in addition to cracks, a small amount of wear debris accumulation and large pores are observed, and the results are similar to those of the P-AO sample. This indicates that the S-AO sample is mainly dominated by fatigue wear and adhesive wear. It can be seen from Fig. 8e, after a 20 min reciprocating friction test of the only anodized without aging sample, a large number of cracks, large debris accumulation areas and some small holes appear on the surface (as shown in Fig. 8e), which is similar to that of P-AO sample. This is because the sample has not been aged treatment, the strength of the matrix is low, and the matrix cannot play a good support in the friction process, resulting in rapid adhesive wear. Although the strength at the interface of S-AO sample is also very low, the softening zone is only within the range of 50 nm of the membrane base interface, and the whole matrix material can play a good supporting role. The specific matrix hardness values are shown in Table 2.

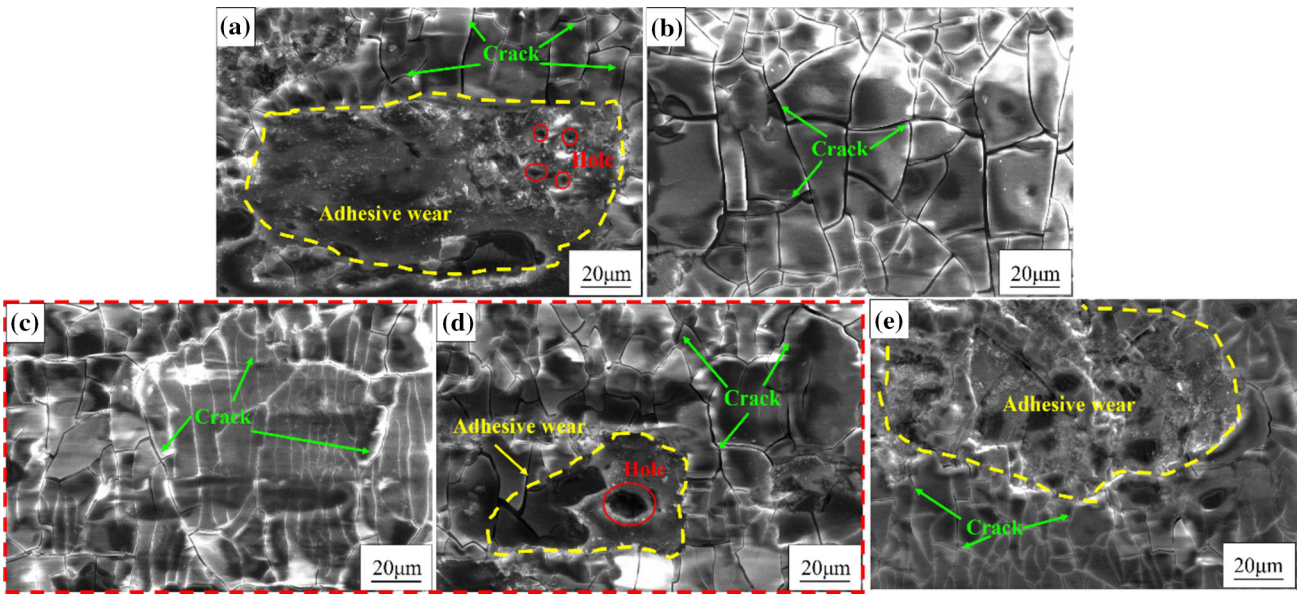

Figure 8 SEM images of friction morphologies. **a**, **b** and **e** the friction morphologies of the P-AO, U-AO and anodized without aging samples after rubbing for 20 min, respectively; **c** and **d** the friction morphologies of the S-AO samples after rubbing 5 and 20 min, respectively.

Table 2 Matrix hardness of anodized samples (Hv)

Sample	1#	2#	3#	Average value
P-AO	115.6	117.2	115.3	116.0
U-AO	116.3	115.5	116.7	116.2
S-AO	115.8	115.6	116.1	115.8
Only anodized	71.3	72.7	70.5	71.5

Discussion

We found that the anodized AA6082 alloy has the best friction resistance when the Mg exists in atomic clusters or GP zones before anodization, follow by the supersaturated solid solution, and in the last is the β″ phase. According to the above analysis and characterization, the thicknesses of the three oxide films are similar (as shown in Fig. 3). Studies have shown that the anodic oxide film exhibits an amorphous structure [38], and the elastic modulus of the anodic oxide film is not directly related to the oxidation conditions [39], in the range of 122–140 GPa [40, 41]. In addition, the state of Mg before anodization does not affect the overall structure of the aluminum matrix, but only affects the structure at the interface. Therefore, it can be determined that the difference in the film/aluminum alloy interface structure is the main reason for the difference in the friction properties of the three oxide films.

It can be seen from the "TEM images of the film/matrix interface" section, especially the interface HRTEM image of the S-AO sample, anodizing would cause the consumption of Mg on the surface of the aluminum alloy. Research shows that Mg in the β″ phase is oxidized to Mg^{2+} species during anodizing due to its relatively high activity [24, 37], which leads to the consumption of the β″ phase. To explore the effect of the consumption of the precipitates on the structure of the film/aluminum alloy interface during the anodization process, the regions with and without the precipitates at the film/aluminum alloy interface of P-AO sample were observed and analyzed as shown in Fig. 9a and b, respectively. As seen in Fig. 9f and g, these areas underwent IFFT processing using the $<110>_{Al}$ diffraction spots. It is possible to find some line defects around the β″ phase at the film/aluminum alloy interface, but some line defects are also present in areas without the β″ phase. Different from the P-AO sample, the Mg in the U-AO and S-AO samples does not exist in the state of precipitates before anodization. For the U-AO sample, the regions with and without the precipitated phase (as shown in Fig. 9c, d, respectively) were analyzed. Figure 9h and i shows the IFFT images acquired from Fig. 9c and d, respectively. It can be seen that when there is a β″ phase at the film/aluminum alloy interface, there are line defects around the precipitates, and the result is consistent with the P-AO sample. However, when there is no β″ phase at the

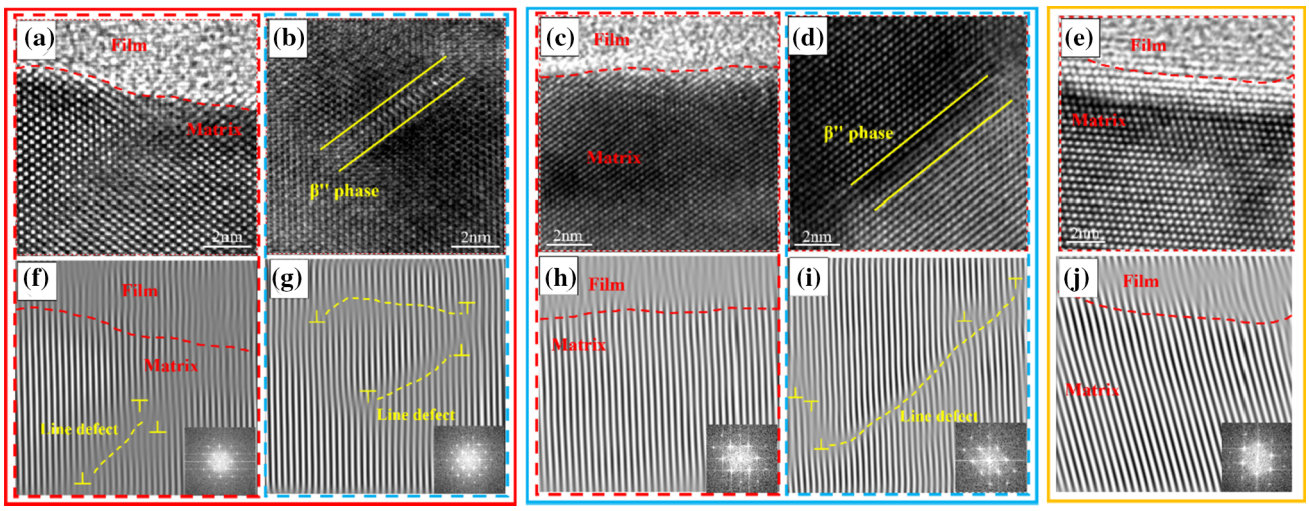

Figure 9 **a**, **c** and **e** HRTEM images of P-AO, U-AO and S-AO samples without precipitation at the film/matrix interface, respectively; **f**, **h** and **j** processed by $<110>_{Al}$ IFFT corresponding to (**a**), (**c**) and (**e**), respectively; **b** and **d** HRTEM images of P-AO and U-AO samples with precipitation at the film/matrix interface, respectively; **g** and **i** processed by $<110>_{Al}$ IFFT corresponding to (**b**) and (**d**), respectively.

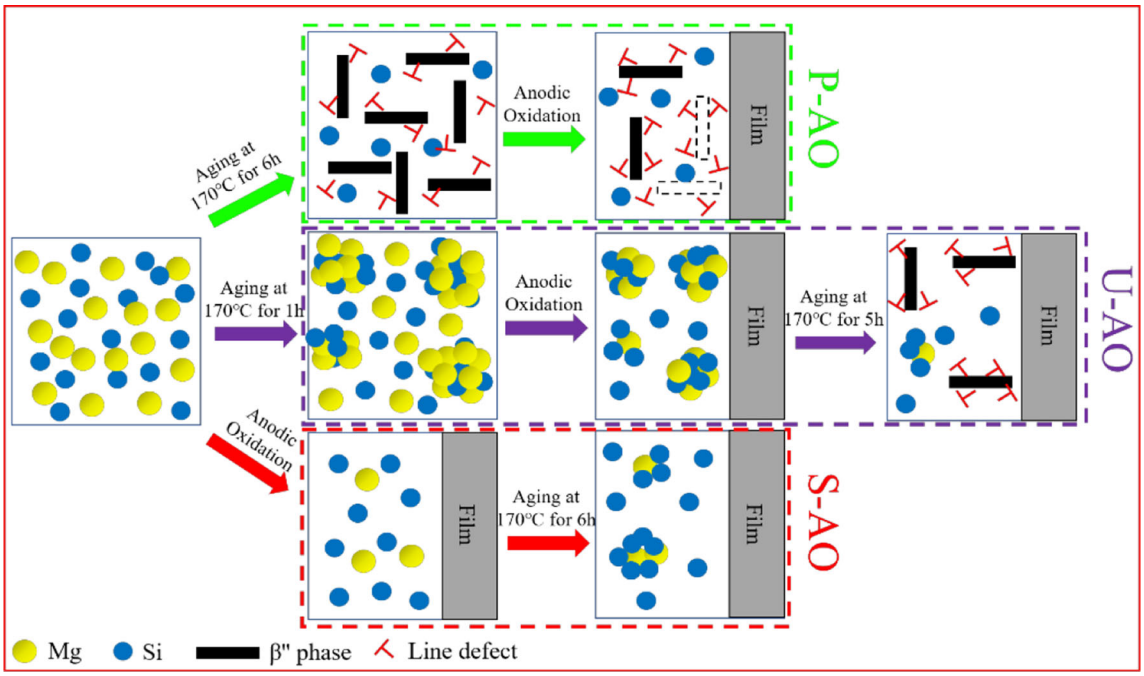

Figure 10 Schematic diagram of anodic oxidation growth process.

film/aluminum alloy interface of the U-AO sample, the atoms in the aluminum alloy matrix show a highly ordered arrangement. For the S-AO sample, since no β″ phase is found at the film/aluminum alloy interface, there are no line defects and the atoms at the film/base interface presented a highly ordered arrangement (as shown in Fig. 9j).

To sum up, the state of Mg before anodization mainly affects the consumption form of Mg during anodization and the formation of β″ phase during subsequent heat treatment. According to the above results, a schematic diagram (as shown in Fig. 10) is used to express the evolution of the interface structure during anodization. When Mg exists in β″ phase before anodization, some β″ phases would be dissolved with the consumption of Mg during anodization, and the surrounding line defects would be retained. So the strength of the aluminum matrix at the interface is reduced due to the consumption of the β″ phase during anodization, and the residual line defects around the consumed precipitates are more prone to stress concentration under the action of cyclic shear stress, which accelerates the occurrence of adhesive wear. The wear debris dropped by adhesive wear continues to participate in the counter-grinding. During the counter-grinding process, the large pieces of wear debris are partially ground under the action of the extrusion force (normal stress), and some are directly embedded in the matrix [42, 43]. However, the hardness of the large abrasive chips embedded in the matrix is much higher than that of the matrix, which leads to the deformation of the matrix and the generation of holes during the crushing process, which leads to a rapid increase in the friction coefficient of the P-AO sample.

When Mg exists in atomic clusters or GP zones before anodization, although the consumption of Mg also occurs during the anodization process, some atomic clusters or GP zones that meet the conditions would be transformed to the β″ phase in the subsequent aging process, so line defects would also be introduced around the β″ phase. The part without the precipitates would not undergo lattice distortion so the atoms in this part would be highly ordered. Therefore, under the action of cyclic contact stress, the existence of the β″ phase hinders the slip of line defects, and the ability of the film/aluminum alloy interface to resist shear strain increases, thereby improving the friction and wear resistance of the U-AO specimens.

When Mg exists as a supersaturated solid solution before anodization, no lattice distortion occurs at the film/aluminum alloy interface. It is worth noting that the Mg at this time does not form atomic clusters and is dispersed in the aluminum matrix, which makes the Mg on the surface of the aluminum matrix

exhausted after anodization, so that the β″ phase cannot be formed, which results in increased toughness and decreased strength of the aluminum matrix at the film/aluminum alloy interface. In addition, because the β″ phase cannot be formed at the film/aluminum alloy interface, line defects are avoided (as shown in Fig. 9j) and the stability of the film/aluminum alloy interface is improved. For this reason, the high toughness and high stability of the film/aluminum alloy interface make the S-AO sample free from fatigue and adhesive wear during the reciprocating friction process within 5 min. But the ability to resist shear strain is related to the strength and toughness of the material [44–47]. Although the high toughness and high stability of the film/aluminum alloy interface of the S-AO sample increase the ability to resist fatigue and adhesive wear to a certain extent, the strength of the aluminum matrix at the film/aluminum alloy interface is too low. Therefore, after a certain period of reciprocating friction, the film/aluminum alloy interface still cannot resist the action of cyclic contact stress, resulting in fatigue and adhesive wear, as well as the rapid increase in the friction coefficient, thereby reducing the friction and wear resistance of the S-AO sample.

Conclusion

This work studied the improvement of interface stability and anti-friction performance by adjusting the state of Mg before anodization. The effects of Mg in different states on the film/aluminum alloy interface structure of AA6082 alloy and the corresponding tribological behavior after anodization were systematically investigated. The main conclusions are as follows:

1. The heat treatment state of the aluminum substrate before anodization would not affect the thickness of oxide film, but will change the film/aluminum alloy interface structure.
2. Through the results and analysis, we confirmed that avoiding the precipitation of β″ phase before anodization is beneficial to improve the stability of the film/aluminum alloy interface. At the same time, although the excessive dispersion of Mg could improve the stability of the interface after anodization, it would reduce the strength of the matrix.
3. The existence state of Mg before anodizing has an important influence on the wear performance. The friction resistance of the anodized AA6082 alloy is the best when the Mg in the state of atomic clusters or GP zones, followed by in the state of supersaturated solid solution, and the worst is in the state of β″ phase.

Funding

This study was funded by The National Building Project of Application Demonstration Platform on New Materials Products (Project No. TC190H3ZV/2).

Data availability

The data used to support the findings of this study are available from the corresponding author upon request.

Declarations

Conflict of interest The authors declare that they have no conflict of interest.

References

[1] Ramesh A, Akram W, Mishra SP, Cannon AH, Polycarpou AA, King WP (2013) Friction characteristics of microtextured surfaces under mixed and hydrodynamic lubrication. Tribol Int 57:170–176

[2] Zhu L, Qiu F, Zou Q, Han X, Shu SL, Yang HY, Jiang QC (2021) Multiscale design of α-Al, eutectic silicon and Mg_2Si phases in Al–Si–Mg alloy manipulated by in situ nanosized crystals. Mater Sci Eng A 802:140627

[3] Madhavi Y, Rama Krishna L, Narasaiah N (2021) Corrosion-fatigue behavior of micro-arc oxidation coated 6061–T6 Al alloy. Int J Fatigue 142:105965

[4] Liew KW, Chia SY, Kok CK, Low KO (2013) Evaluation on tribological design coatings of Al_2O_3, Ni–P–PTFE and MoS_2 on aluminium alloy 7075 under oil lubrication. Mater Des 48:77–84

[5] Hu LF, Chen DM, Shi FR, Chen SP (2016) Effect of AlSiFe on the anodizing process of 6063 aluminum. Surf Interface Anal 48:1299–1304

[6] Li YW, Chen YL, Qiu MX, Yu HY, Zhang XH, Sun XW, Chen R (2016) Preparation of aluminum nanomesh thin

films from an anodic aluminum oxide template as transparent conductive electrodes. Sci Rep 6:20114

[7] Wu DQ, Ma LW, Liu B, Zhang DW, Minhas B, Qian HC, Terryn HA, Mol JMC (2021) Long-term deterioration of lubricant-infused nanoporous anodic aluminum oxide surface immersed in NaCl solution. J Mater Sci Technol 64:57–65

[8] Chi CS, Lee JH, Kim I, Oh HJ (2015) Effects of microstructure of aluminum substrate on ordered nanopore arrays in anodic alumina. J Mater Sci Technol 31:751–758

[9] Aerts T, Dimogerontakis T, De Graeve I, Fransaer J, Terryn H (2007) Influence of the anodizing temperature on the porosity and the mechanical properties of the porous anodic oxide film. Surf Coat Technol 201:7310–7317

[10] Frantila-Apachitei LE, Duszczyk J, Katgerman L (2003) Vickers microhardness of AlSi(Cu) anodic oxide layers formed in H_2SO_4 at low temperature. Surf Coat Technol 165:309–315

[11] Wang Y, Xia L, Ding J, Yuan N (2015) Effect of pore depth on tribological behavior of anodic alumina films under nano-thin film lubrication. Colloid Surf A 468:226–233

[12] Buijnsters JG, Zhong R, Tsyntsaru N, Celis JP (2013) Surface wettability of macro-porous anodized aluminum oxide. ACS Appl Mater Interfaces 5:3224–3233

[13] Ding JN, Zhu Y, Yuan NY, Ding GQ (2011) Thermal driving fast fabrication of porous anodic alumina. J Electrochem Soc 158:C410–C415

[14] Wang Y, Xia L, Ding JN, Yuan NY, Zhu YY (2013) Tribological behaviors of lubricants modified nanoporous anodic alumina film. Tribol Lett 49:431–437

[15] Lee GS, Choi JH, Choi YC, Bu SD, Lee YZ (2011) Tribological effects of pores on an anodized Al alloy surface as lubricant reservoir. Curr Appl Phys 11:S182–S186

[16] Skeldon P, Wang HW, Thomson GE (1997) Formation and characterization of self-lubricating MoS_2 precursor films on anodized aluminium. Wear 206:187–196

[17] Zhang WJ, Zhang D, Le YK, Li L, Ou B (2008) Fabrication of surface self-lubricating composites of aluminum alloy. Appl Surf Sci 255:2671–2674

[18] Takaya M, Hashimoto K, Toda Y, Maejima M (2003) Novel tribological properties of anodic oxide coating of aluminum impregnated with iodine compound. Surf Coat Technol 169–170:160–162

[19] Kim H, Kim D, Lee W, Cho SJ, Hahn JH, Ahn HS (2010) Tribological properties of nanoporous anodic aluminum oxide film. Surf Coat Technol 205:1431–1437

[20] Hu NN, Ge SR, Fang L (2011) Tribological properties of nano-porous anodic aluminum oxide template. J Cent South Univ Technol 18:1004–1008

[21] Dervishi E, McBride M, Edwards R, Gutierrez M, Li N, Buntyn R, Hooks DE (2022) Mechanical and tribological properties of anodic Al coatings as a function of anodizing conditions. Surf Coat Technol 444:128652

[22] Bensalah W, Elleuch K, Feki M, Wery M, Ayedi HF (2009) Mechanical and abrasive wear properties of anodic oxide layers formed on aluminium. J Mater Sci Technol 25:508–512

[23] Bensalah W, Elleuch K, Feki M, DePetris-Wery M, Ayedi HF (2009) Comparative study of mechanical and tribological properties of alumina coatings formed on aluminium in various conditions. Mater Des 30:3731–3737

[24] Miera MSD, Curioni M, Skeldon P, Thompson GE (2010) The behaviour of second phase particles during anodizing of aluminium alloys. Corros Sci 52:2489–2497

[25] Wang Y, Liu ZK, Chen LQ, Wolverton C (2007) First-principles calculations of β″-Mg_5Si_6/α-Al interfaces. Acta Mater 55:5934–5947

[26] Ninive PH, Strandlie A, Gulbrandsen-Dahl S, Lefebvre W, Marioara CD, Andersen SJ, Friis J, Holmestad R, Løvvik OM (2014) Detailed atomistic insight into the β″ phase in Al–Mg–Si alloys. Acta Mater 69:126–134

[27] Vissers R, van Huis MA, Jansen J, Zandbergen HW, Marioara CD, Andersen SJ (2007) The crystal structure of the β′ phase in Al–Mg–Si alloys. Acta Mater 55:3815–3823

[28] Weng YY, Ding LP, Xu YQ, Jia ZH, Sun QC, Chen FC, Sun XY, Cong Y, Liu Q (2021) Effect of in addition on the precipitation behavior and mechanical property for Al–Mg–Si alloys. J Alloys Compd 895:162685

[29] Weng YY, Ding LP, Jia ZH, Liu Q (2021) Effect of combined addition of Ag and Cu on the precipitation behavior for an Al–Mg–Si alloy. Mater Charact 171:110736

[30] Edwards GA, Stille K, Dunlop GL, Couper MJ (1998) The precipitation sequence in Al–Mg–Si alloys. Acta Mater 46:3893–3904

[31] Zhu WB, Deng YL, Guo XB (2022) Influence of adjusting the anodizing and aging sequences on the microstructure, fatigue property and corrosion resistance of anodized AA6082 alloys. Mater Charact 189:111941

[32] Zhu WB, Deng YL, Zhang Z, Tan GW, Guo XB (2022) Effect of tensile stress response for oxide films on the fatigue failure behavior of anodized AA6082 alloys. Mater Sci Eng A 850:143552

[33] Rateick RG, Griffith RJ, Hall DA, Thompson KA (2005) Relationship of microstructure to fatigue strength loss in anodised aluminium–copper alloys. Mater Sci Technol 21:1227–1235

[34] Monsalve A, Paez M, Toledano M, Artigas A, Sepulveda Y, Valencia YN (2007) S-N-P curves in 7075 T7351 and 2024

T3 aluminium alloys subjected to surface treatments. Fatigue Fract Eng Mater Struct 30:748–758

[35] Buha J, Lumley RN, Crosky AG, Hono K (2007) Secondary precipitation in an Al–Mg–Si–Cu alloy. Acta Mater 55:3015–3024

[36] Li H, Mao QZ, Wang ZX, Miao FF, Fang BJ, Song RG, Zheng ZQ (2014) Simultaneously enhancing the tensile properties and intergranular corrosion resistance of Al–Mg–Si–Cu alloys by a thermo-mechanical treatment. Mater Sci Eng A 617:165–174

[37] Ma Y, Zhou X, Wang J, Thompson GE, Huang W, Nilsson JO, Gustavsson M, Crispin A (2014) Discoloration of anodized AA6063 aluminum alloy. J Electrochem Soc 161:C321–C320

[38] Sola R, Tonelli L, Shashkov P, Bogdanoff TH, Martini C (2020) Anodizing of AA6082-T5 by conventional and innovative treatments: microstructural characterization and dry sliding behaviour. Wear 458–459:203423

[39] Bensalah W, Depetris-Wery M, Ayedi HF (2016) Young's modulus of anodic oxide layers formed on aluminum in sulphuric acid bath. Mater Lett 179:82–85

[40] Alcalá G, Skeldon P, Thompson GE, Mann AB, Habazaki H, Shimizu K (2002) Mechanical properties of amorphous anodic alumina and tantala films using nanoindentation. Nanotechnology 13:451–455

[41] Alcalá G, Mato S, Skeldon P, Thompson GE, Mann AB, Habazaki H, Shimizu K (2003) Mechanical properties of barrier-type anodic alumina films using nanoindentation. Surf Coat Technol 173:293–298

[42] Zheng D, Zhu S, Wang F (2006) Oxidation and hot corrosion behavior of a novel enamel-Al_2O_3 composite coating on K38G superalloy. Surf Coat Technol 200:5931–5936

[43] Chen MH, Shen ML, Zhu SL, Wang FH (2013) Comparative study of interfacial reaction between superalloy substrate and glass coating with and without alumina particles incorporation. Appl Surf Sci 271:228–233

[44] Abe O, Ohwa Y (2004) Oxidation of NiAl/Al_2O_3 composites for controlled development of surface layers and toughening. Solid State Ionics 172:553–556

[45] Wang HL, Zhang S, Li YB, Sun D (2008) Bias effect on microstructure and mechanical properties of magnetron sputtered nanocrystalline titanium carbide thin films. Thin Solid Films 516:5419–5423

[46] Wang YX, Zhang S, Lee JW, Lew WS, Sun D, Li B (2013) Toward hard yet tough CrAlSiN coatings via compositional grading. Surf Coat Technol 231:346–352

[47] Ma Y, Yuan F, Yang M, Jiang P, Ma E, Wu X (2018) Dynamic shear deformation of a CrCoNi medium-entropy alloy with heterogeneous grain structures. Acta Mater 148:407–418